# Supplementary Information

## Atomic High-Spin Cobalt(II) Center for Highly Selective Electrochemical CO Reduction to $CH_3OH$

Ding et al.

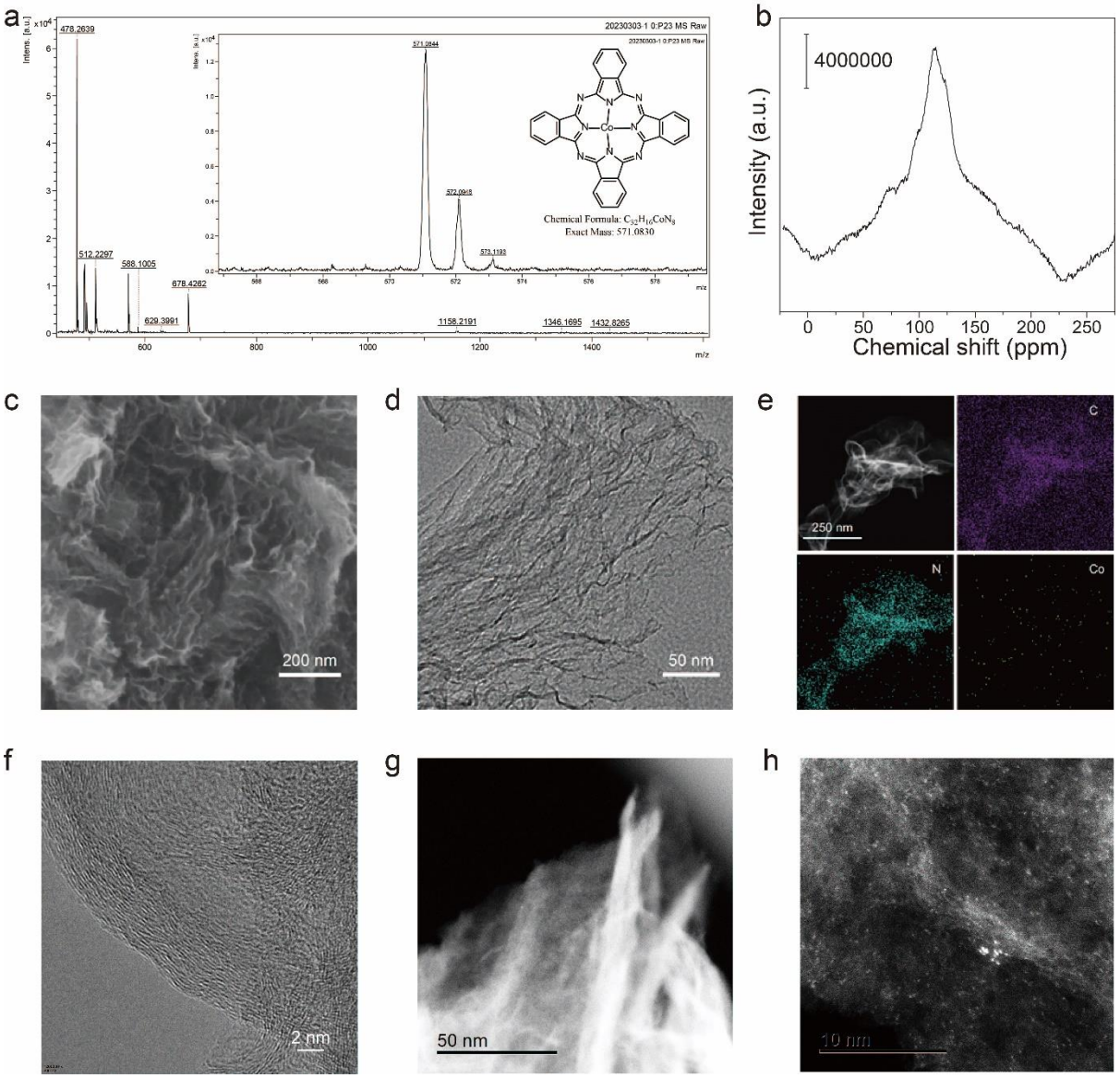


**Figure S1** Morphology and structure characterizations for M-CoPc and M-CoPc-400. a, HR-MS and b, $^{13}C$ NMR spectra for M-CoPc. c, Scanning electron microscopy (SEM) image. d, Transmission electron microscopy (TEM) image. e, Energy dispersive X-ray (EDX) elemental mapping images. f, High-resolution TEM (HR-TEM) image. g, Scanning transmission electron microscopy (STEM) image. h, HAADF-STEM image for M-CoPc-400.

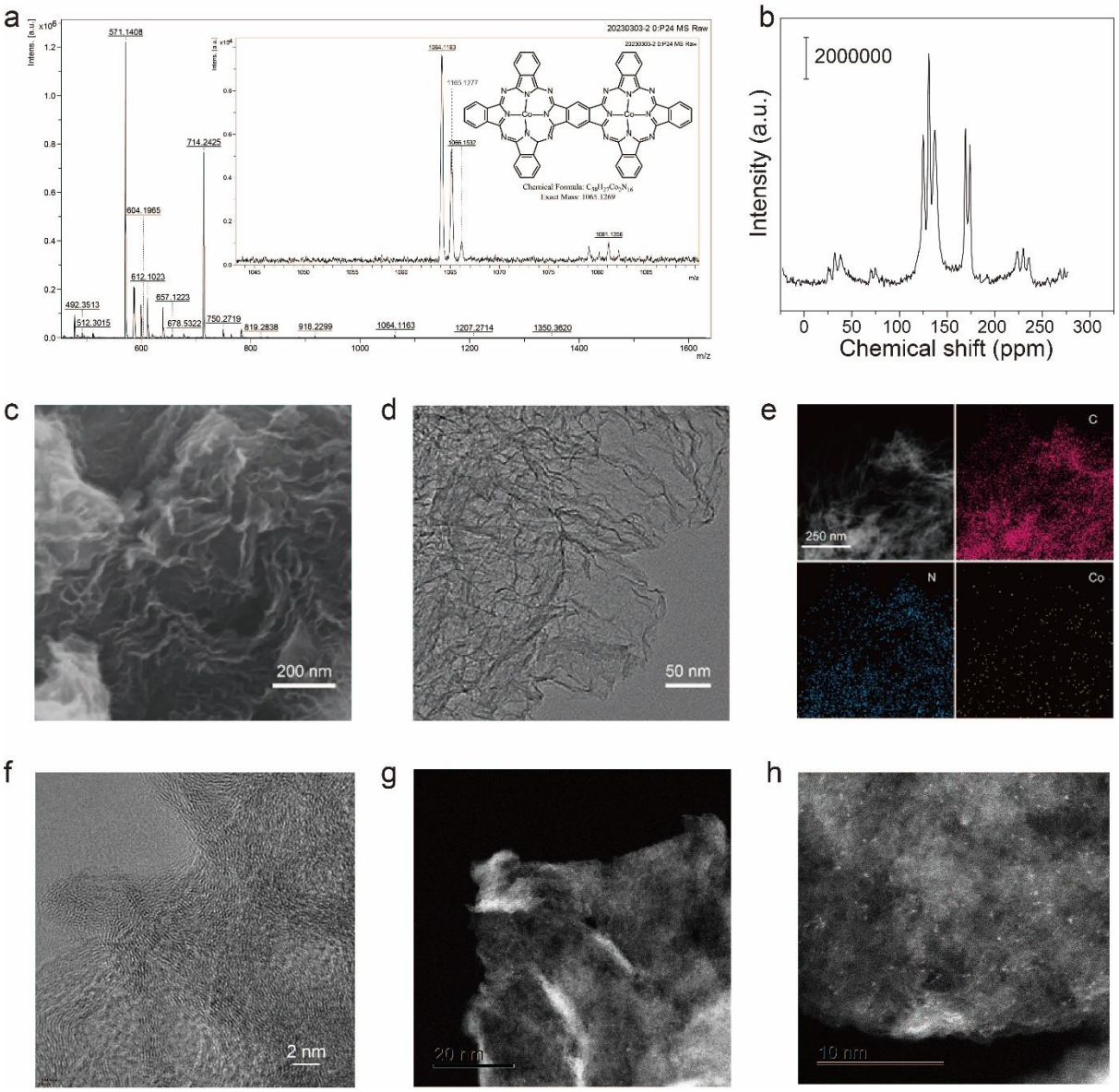


**Figure S2** Morphology and structure characterizations for B-CoPc and B-CoPc-400. a, HR-MS and b, $^{13}C$ NMR spectra for B-CoPc. c, Scanning electron microscopy (SEM) image. d, Transmission electron microscopy (TEM) image. e, Energy dispersive X-ray (EDX) elemental mapping images. f, High-resolution TEM (HR-TEM) image. g, Scanning transmission electron microscopy (STEM) image. h, HAADF-STEM image for B-CoPc-400.

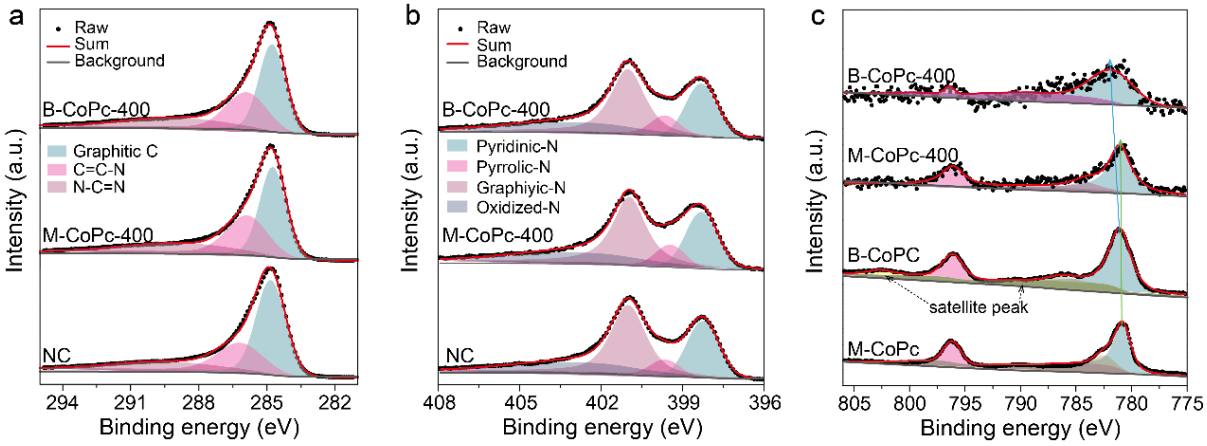


**Figure S3** XPS spectra of M-CoPc-400 and B-CoPc-400: (a) C 1*s*, (b) N 1*s*, and (c) Co 2*p* XPS spectra. The C 1*s* XPS spectra can be deconvoluted into three peaks, corresponding to shake-up features, C=O, and $sp^2$ carbon, respectively. The N 1*s* XPS spectra can be deconvoluted into four peaks, which can be assigned to pyridinic nitrogen, pyrrolic nitrogen, graphitic nitrogen and oxidized nitrogen, respectively. The XPS results show that C and N in M-CoPc-400 and B-CoPc-400 have similar species. After heat treatment, Co 2*p* maintained a similar structure to M-CoPc and B-CoPc. The peak shape was slightly changed, indicating that M-CoPc and B-CoPc interacted with N-doped carbon.

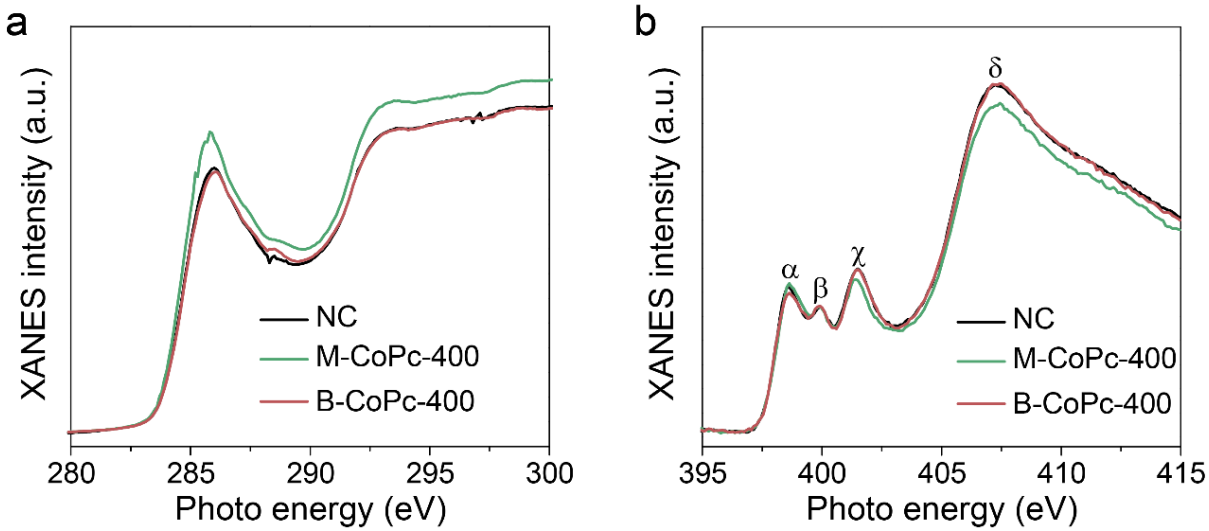


**Figure S4** K-edge XANES spectra for C (a) and N (b) of NC, M-CoPc-400 and B-CoPc-400. One main feature is observed in the pre-edge region at ca. 285.6 eV (C-C). The C-C feature is related to electron transitions from C 1*s* orbital to π*(C=C) orbital, mostly coming from interlayered C=C bond configuration, in agreement with the results from XPS. In the N K-edge XANES spectra, both M-CoPc-400 and B-CoPc-400 display four features at 396.5 eV and 407.8 eV, associated with pyridinic nitrogen (α), pyrrolic nitrogen (β), graphitic nitrogen (γ) and oxidized nitrogen (δ), in line with N 1*s* XPS data.

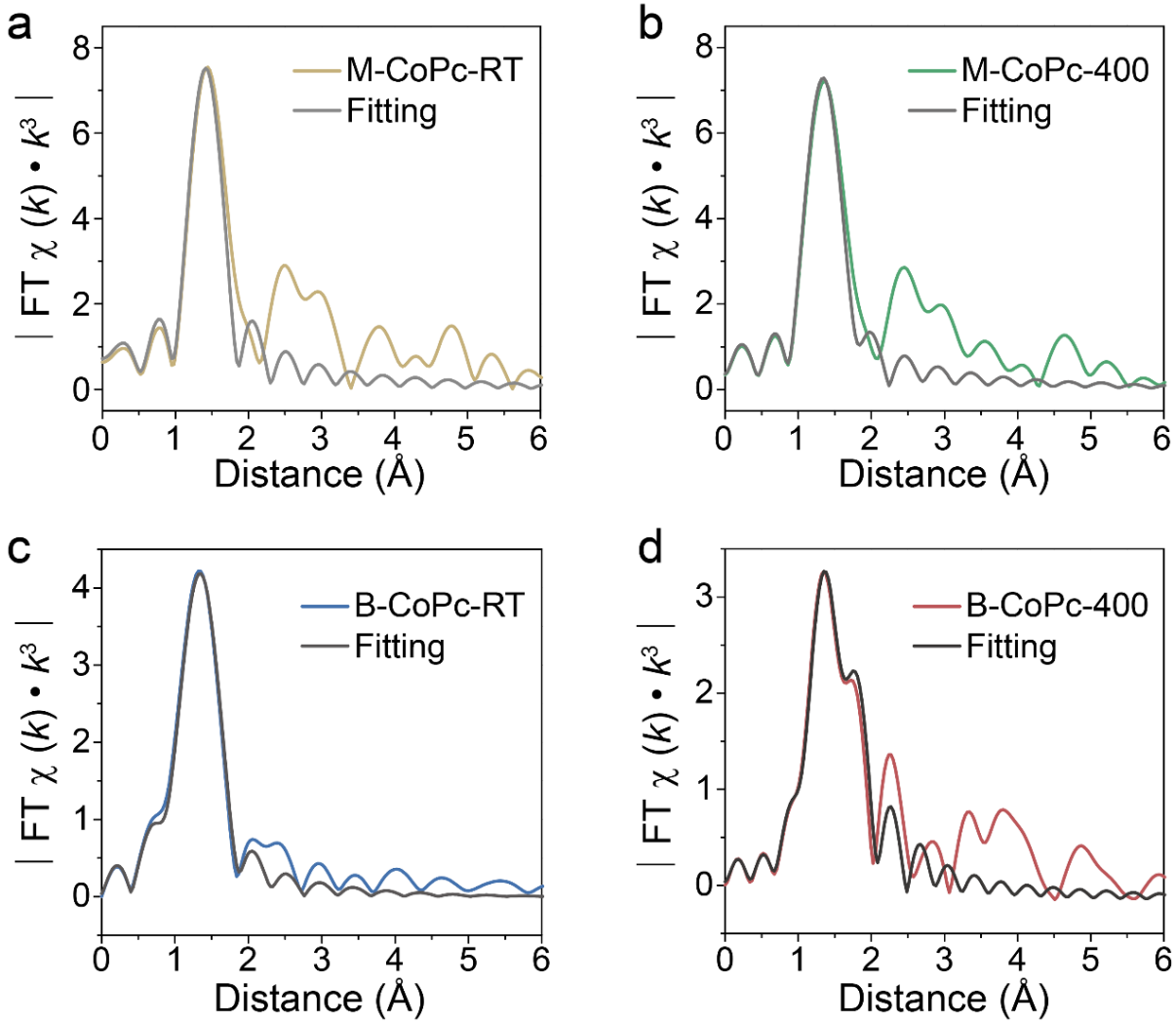


**Figure S5** First-shell (Co-N) fitting of Fourier transformations of EXAFS spectra for M-CoPc-RT (a), M-CoPc-400 (b), B-CoPc-RT (c) and B-CoPc-400 (d). EXAFS spectra were fitted using the FEFF 6.0 code.

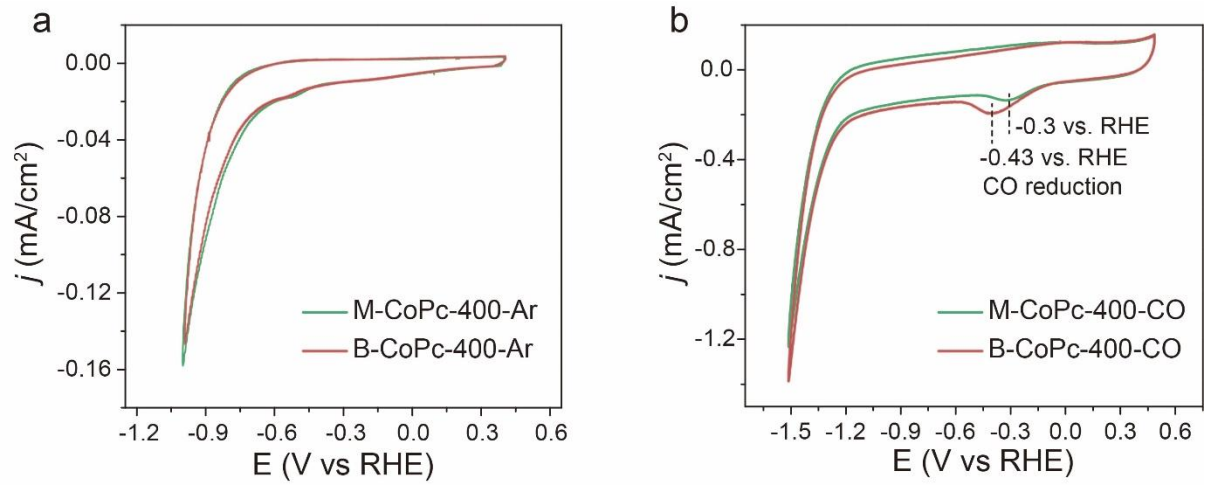


**Figure S6** Cyclic voltammetry curves recorded in Ar-saturated (a) and CO-saturated (b) 0.5 M KOH aqueous solution.

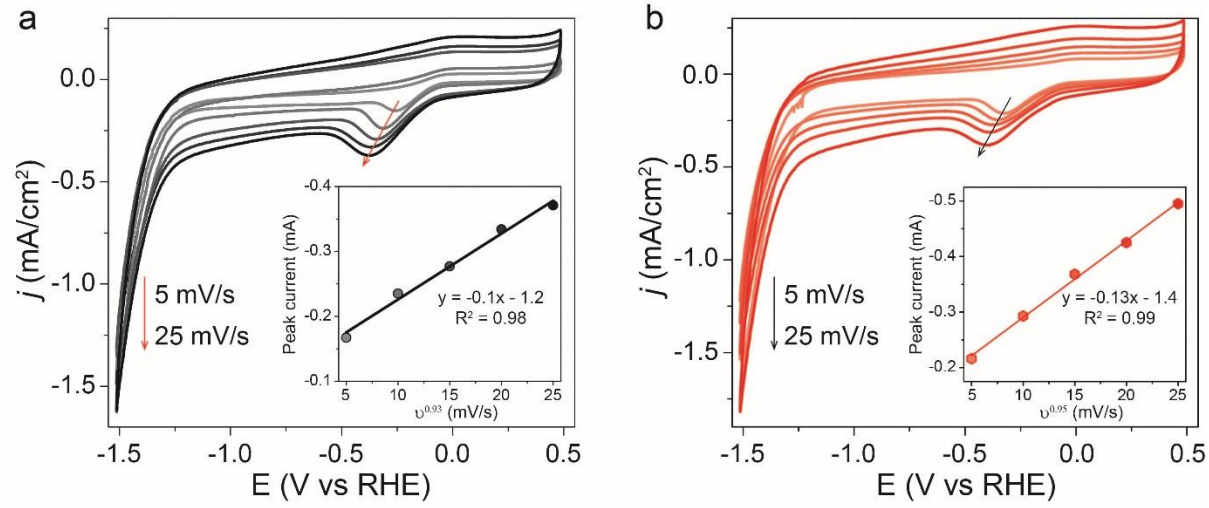


**Figure S7** Cyclic voltammetry curves recorded at a scan rate of 5, 10, 15, 20, and 25 mV/s over (a) M-CoPc-400 and (b) B-CoPc-400 electrode in CO-saturated 0.5M KOH. Generally, the reduction peak current ($I_p$) obeys the power law relation with scan rate (ν): $I_p = a \times v^b$, where $I_P$ is the peak current, a and b are adjustable parameters. The value of b can be estimated from the slope of the log ($I_P$) vs. log (ν) plot. There are two well-defined conditions: if b is close to 1, indicating purely surface reaction-controlled mechanism and b = 0.5, indicating purely diffusion-controlled mechanism. As revealed in the inset of Figure S9a and b, the b value for M-CoPc-400 and B-CoPc-400 are estimated to be ~0.93 and ~0.95, respectively.

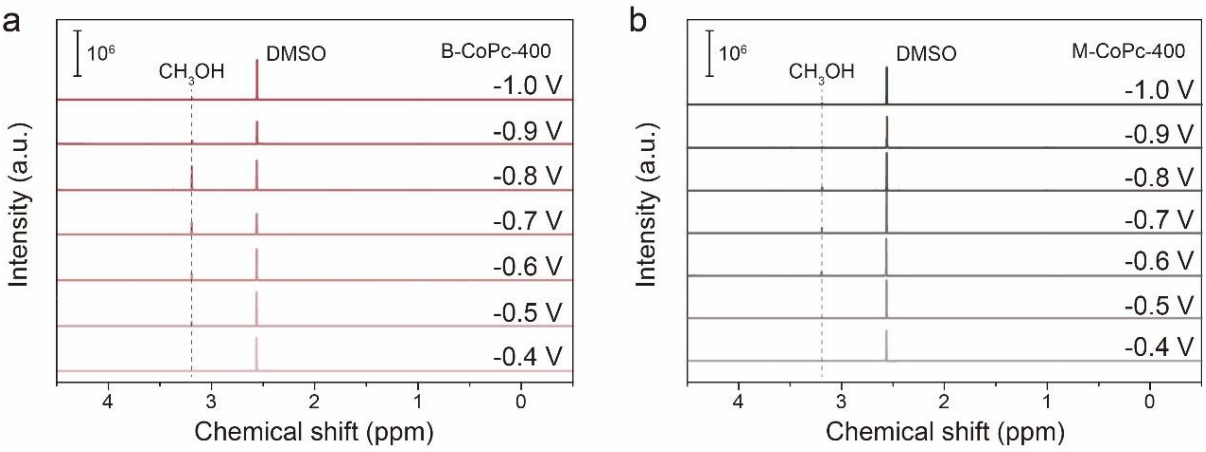


**Figure S8** $^{1}$H 1D NMR spectra of products and DMSO at different potentials (vs. RHE) for B-CoPc-400 (a) and M-CoPc-400 (b), respectively.

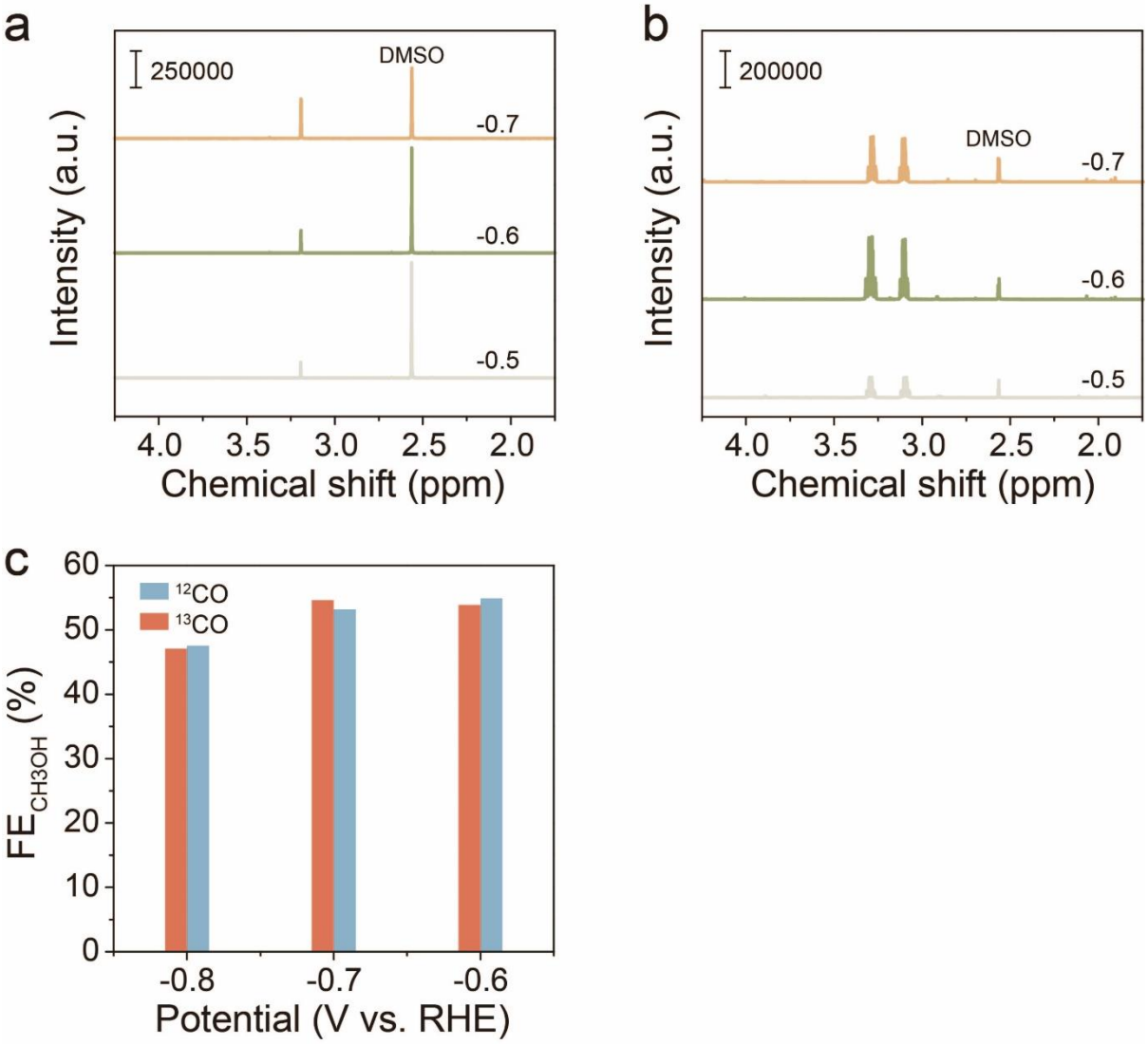


**Figure S9** $^{1}$H 1D NMR spectra of products and DMSO recorded at different potentials (vs. RHE) over M-CoPc-400 (a) and B-CoPc-400 (b). c, Comparison of Faradaic efficiency of $CH_3OH$ with $^{13}CO$ and $^{12}CO$ as the reactant.

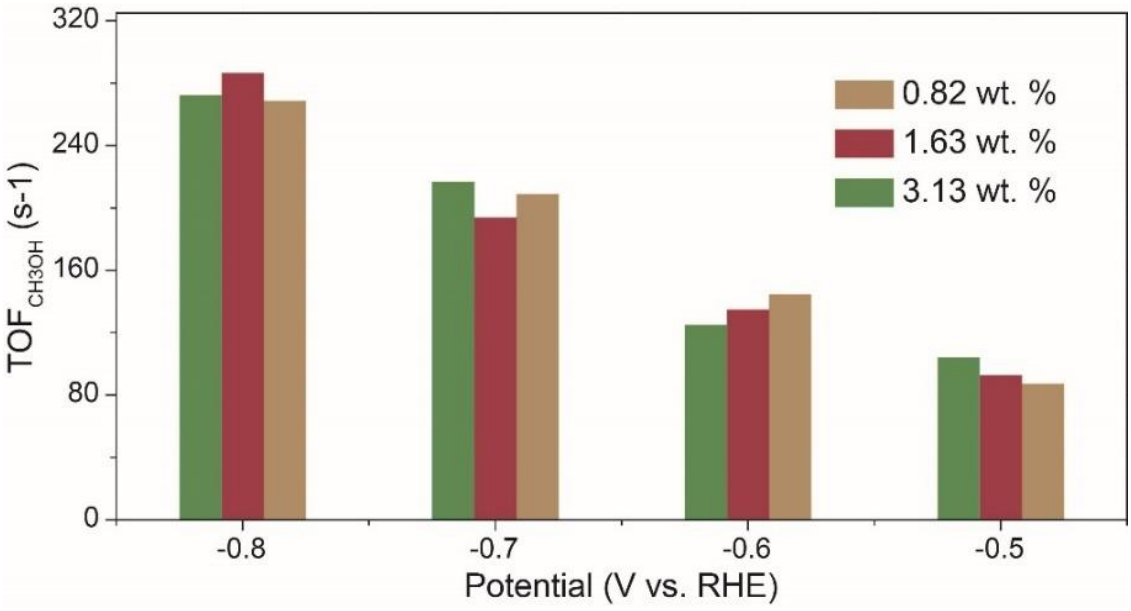


**Figure S10** Potential-dependent product selectivity for CO electroreduction over B-CoPc-400 with different Co loading amount.

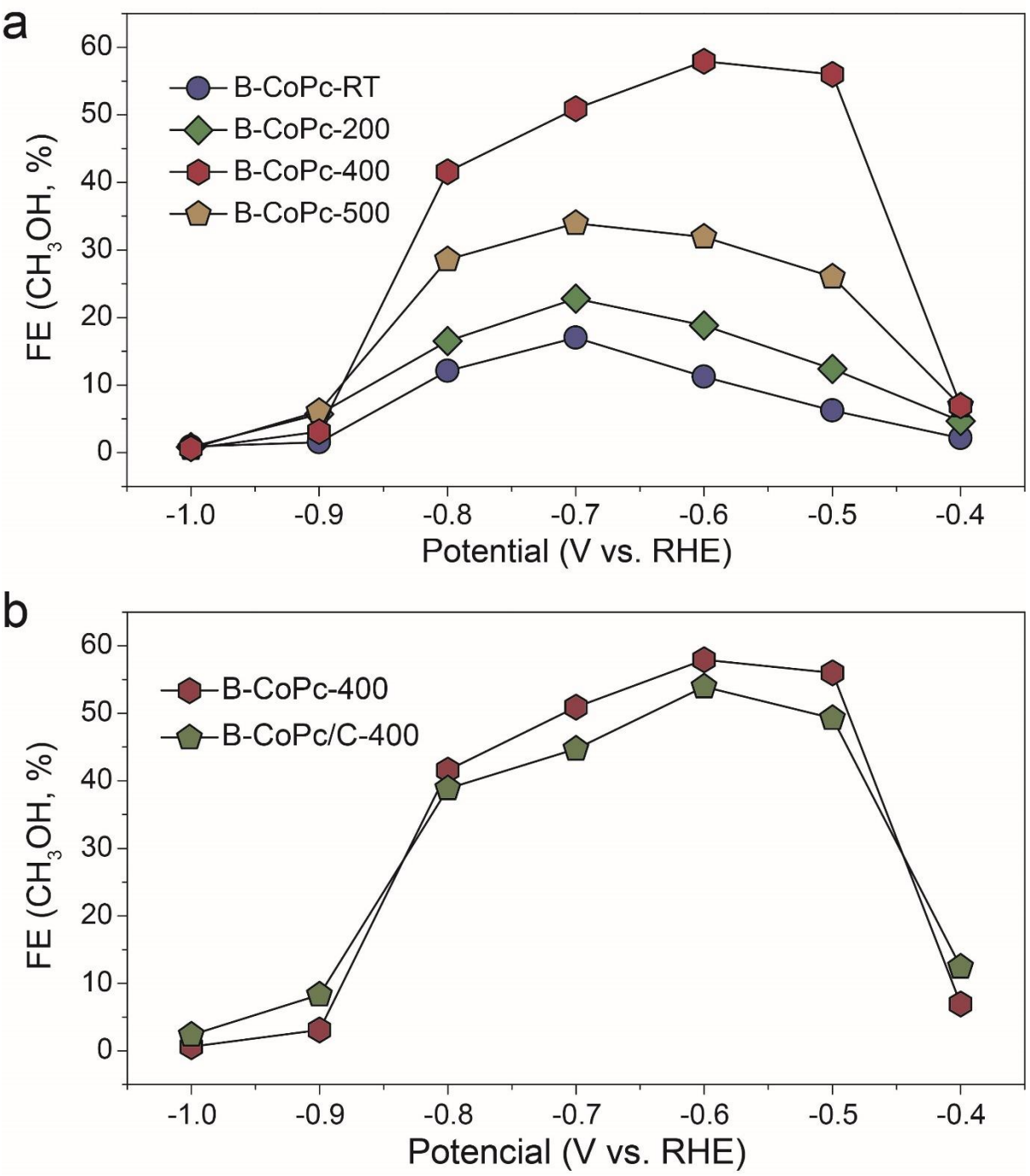


**Figure S11** a, Potential-dependent product selectivity for CO electroreduction catalyzed by B-CoPc-X (X represents treatment temperature). b, Potential-dependent product selectivity for CO electroreduction catalyzed by B-CoPc-400 and B-CoPc/C-400 (B-CoPc/C-400 represents Vulcan carbon black as support to prepare the catalyst).

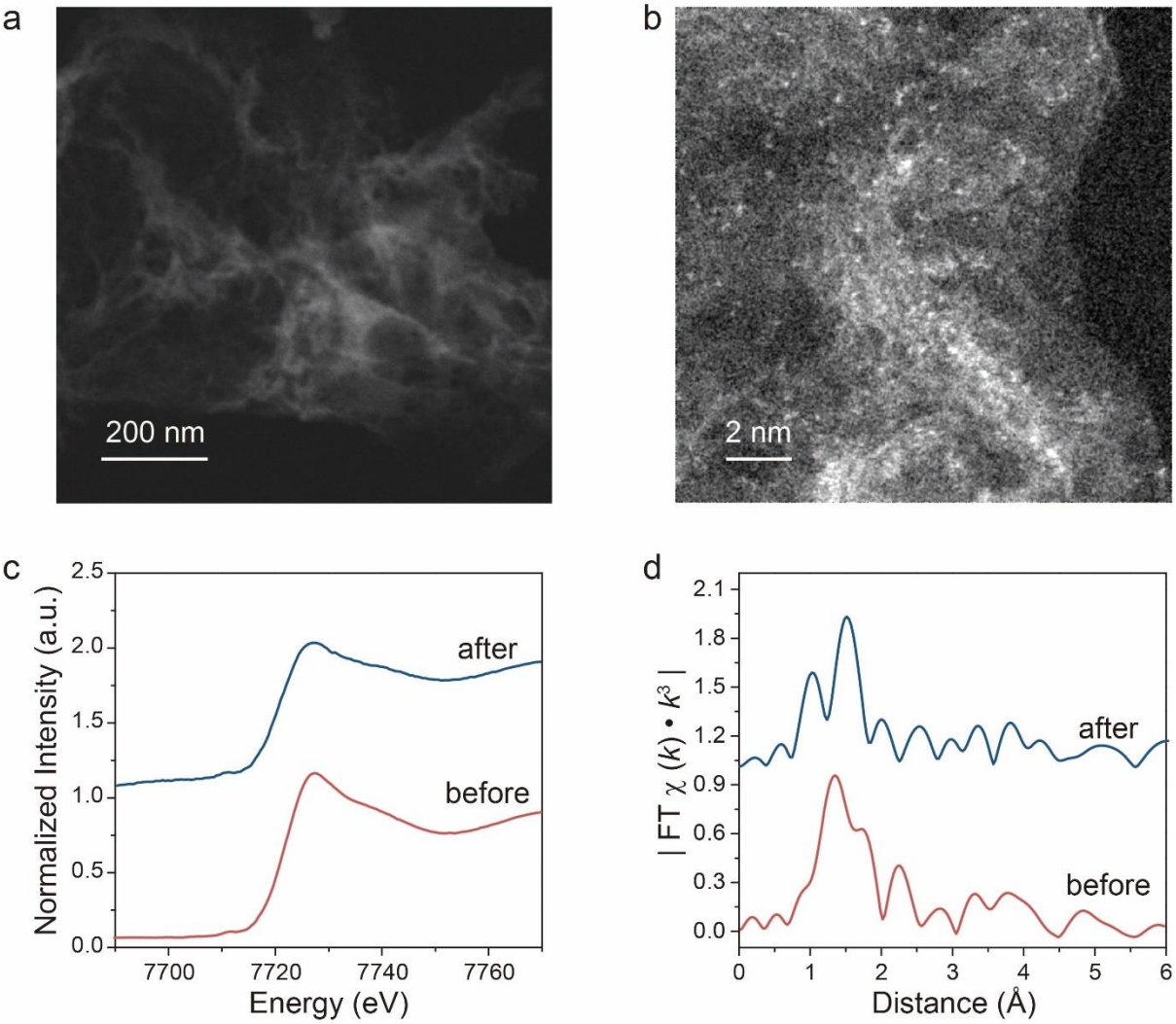


**Figure S12** HRTEM (a) and HADDF-STEM (b) of B-CoPc-400 after CORR. c, Co K-edge XANES spectra for B-CoPc-400 before and after CORR. d, The corresponding Fourier transformation (FT)-EXAFS spectra.

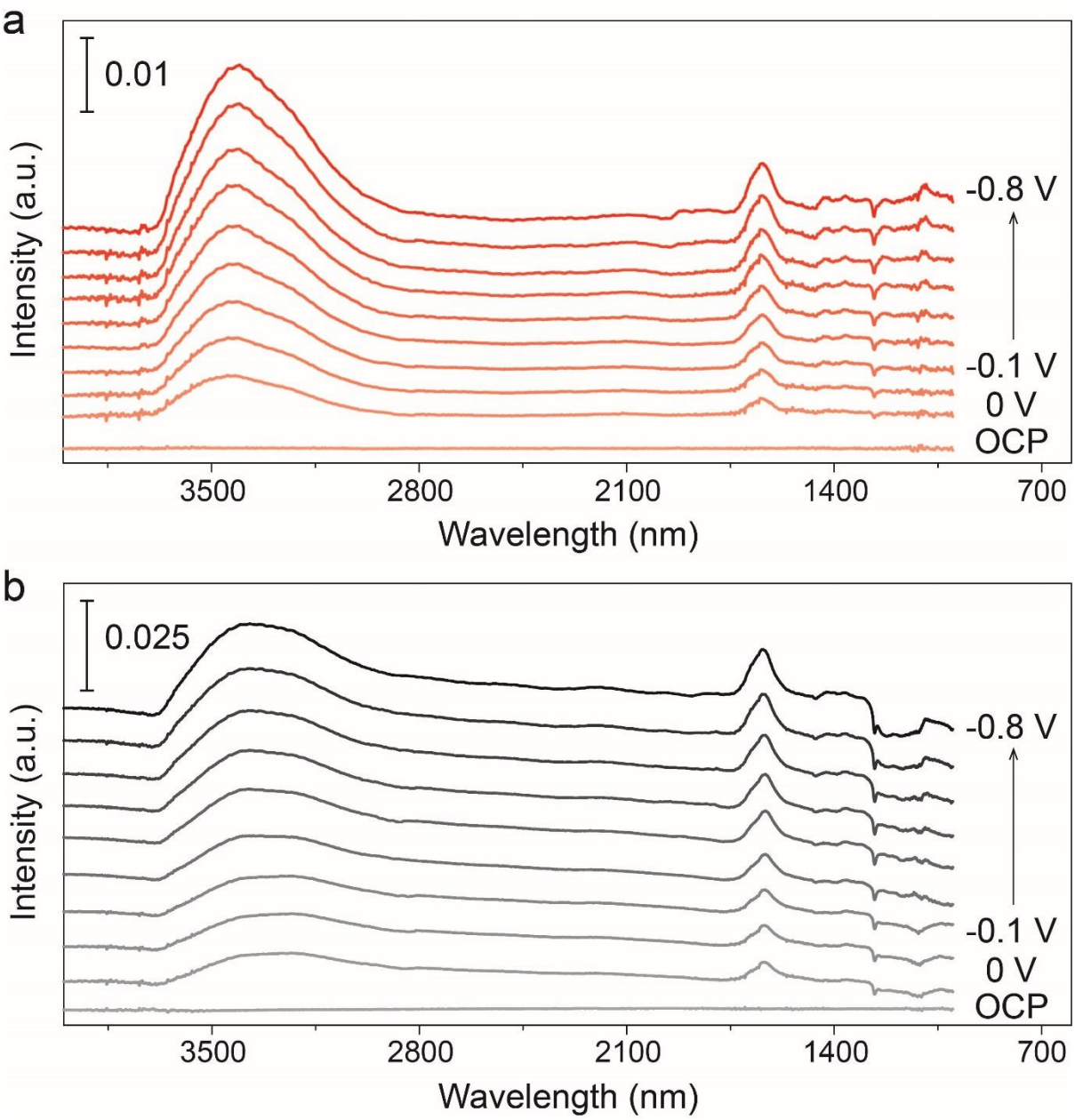


**Figure S13** *Operando* ATR-SEIRAS spectra recorded on M-CoPc-400 (a) and B-CoPc-400 (b) in Ar-saturated 0.5 M KOH.

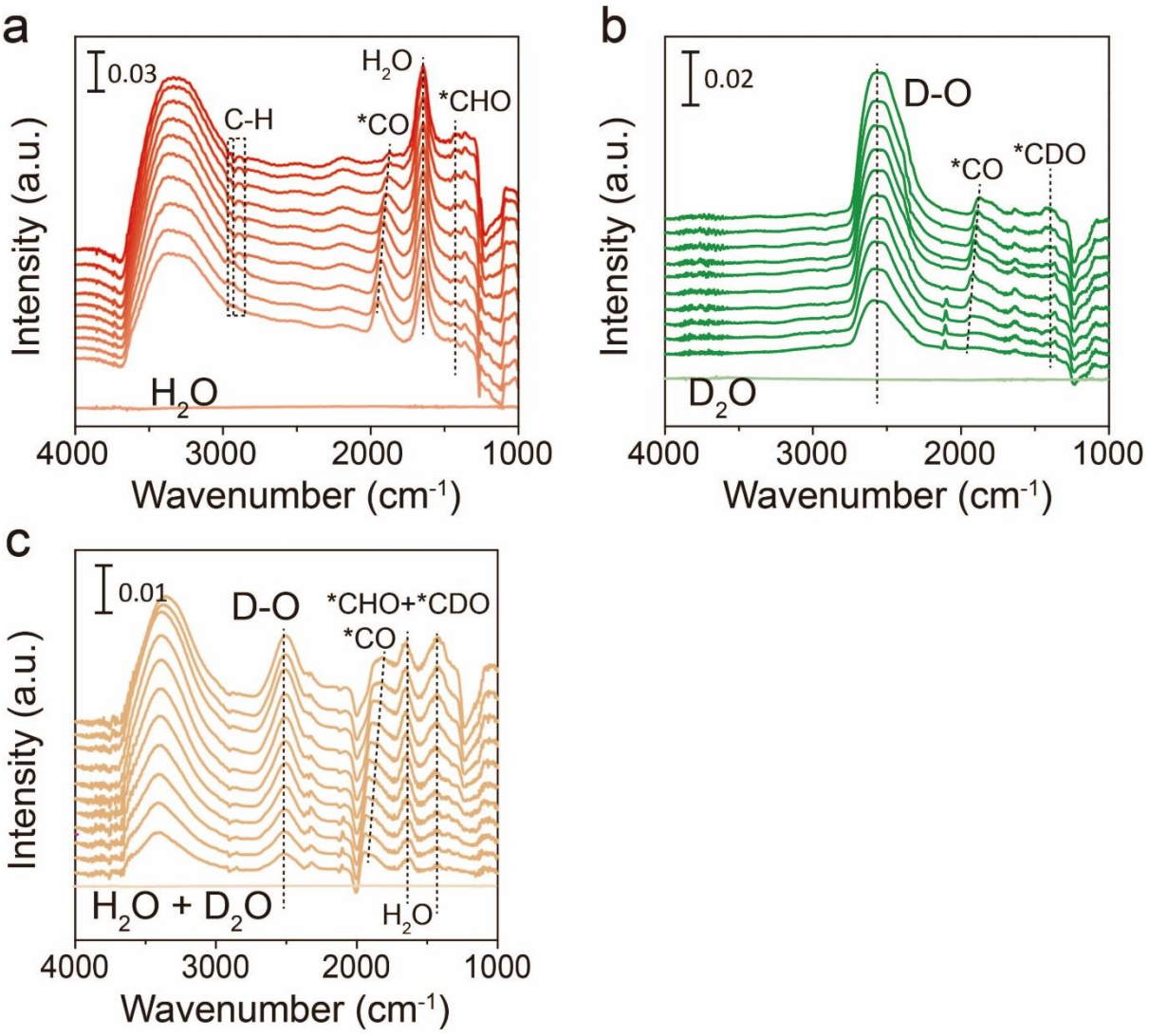


**Figure S14** *Operando* ATR-SEIRAS spectra recorded over B-CoPc-400 in CO-saturated 0.5 M $KHCO_3$ with $H_2O$ (a), $D_2O$ (b), and $H_2O$ + $D_2O$ (c) as solvent.

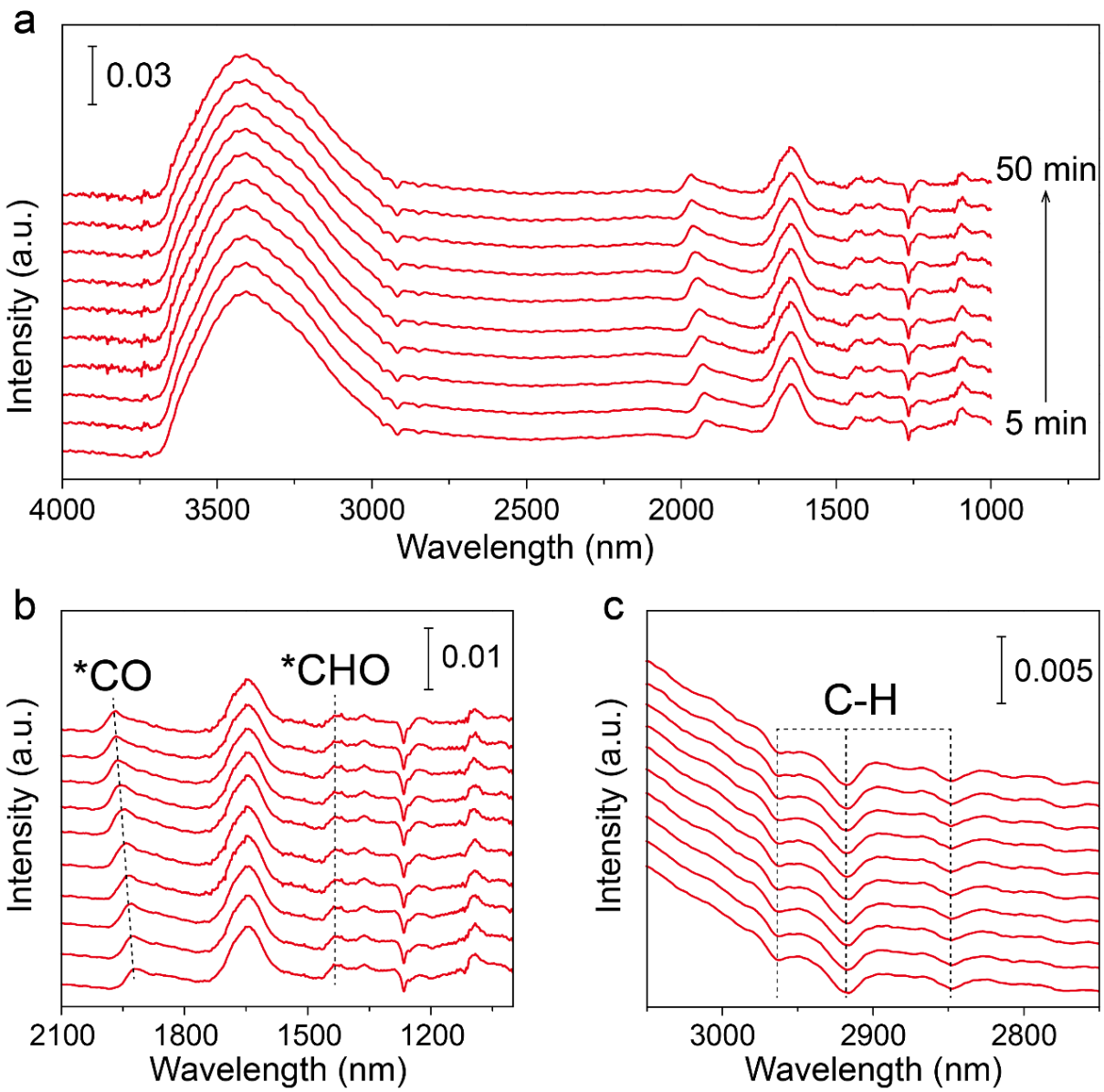


**Figure S15 (a-c)** Time-dependent *operando* ATR-SEIRAS spectra recorded on B-CoPc-400 in CO-saturated 0.5 M KOH.

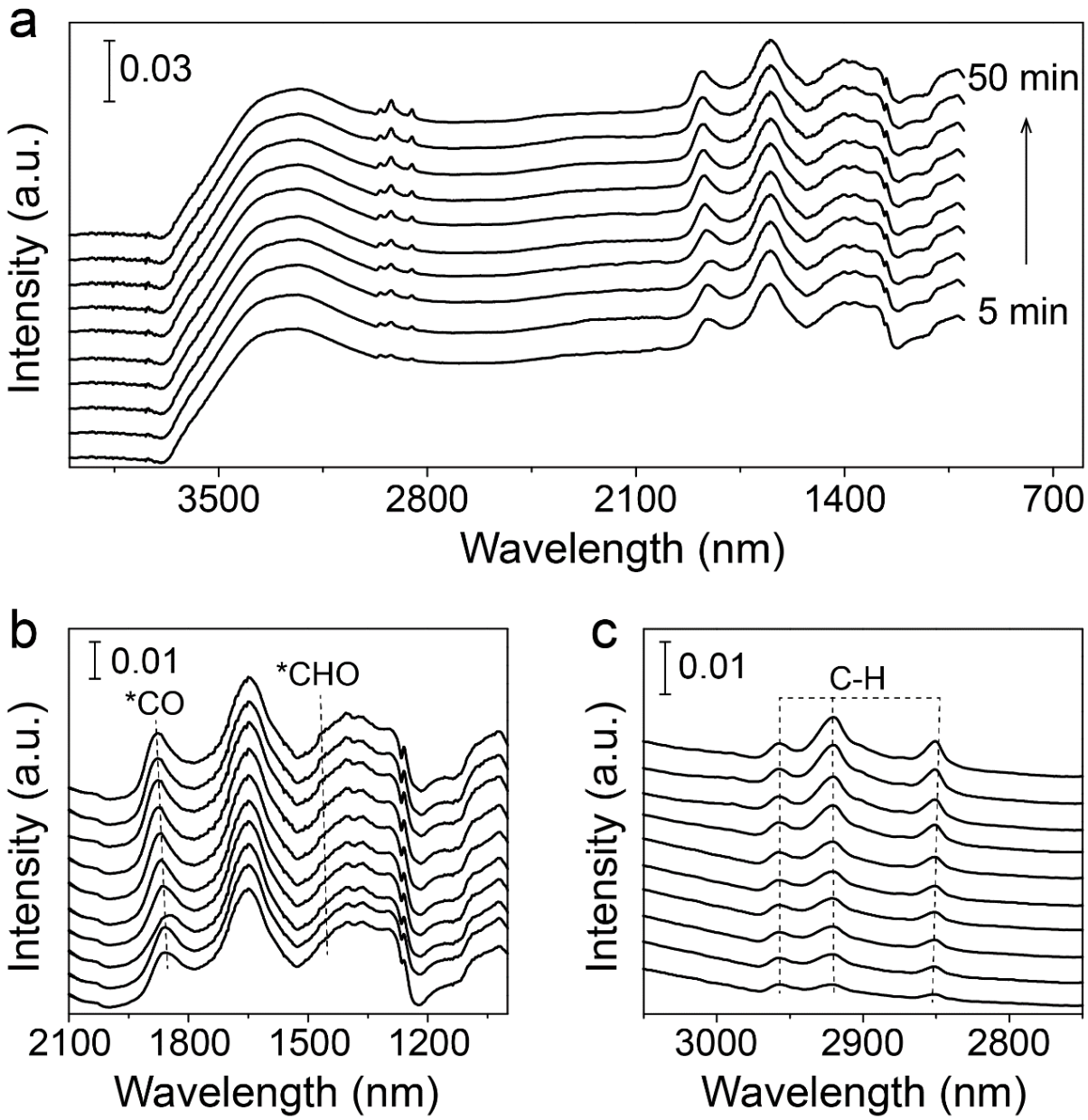


**Figure S16 (a-c)** Time-dependent *operando* ATR-SEIRAS spectra recorded on M-CoPc-400 in CO-saturated 0.5 M KOH.

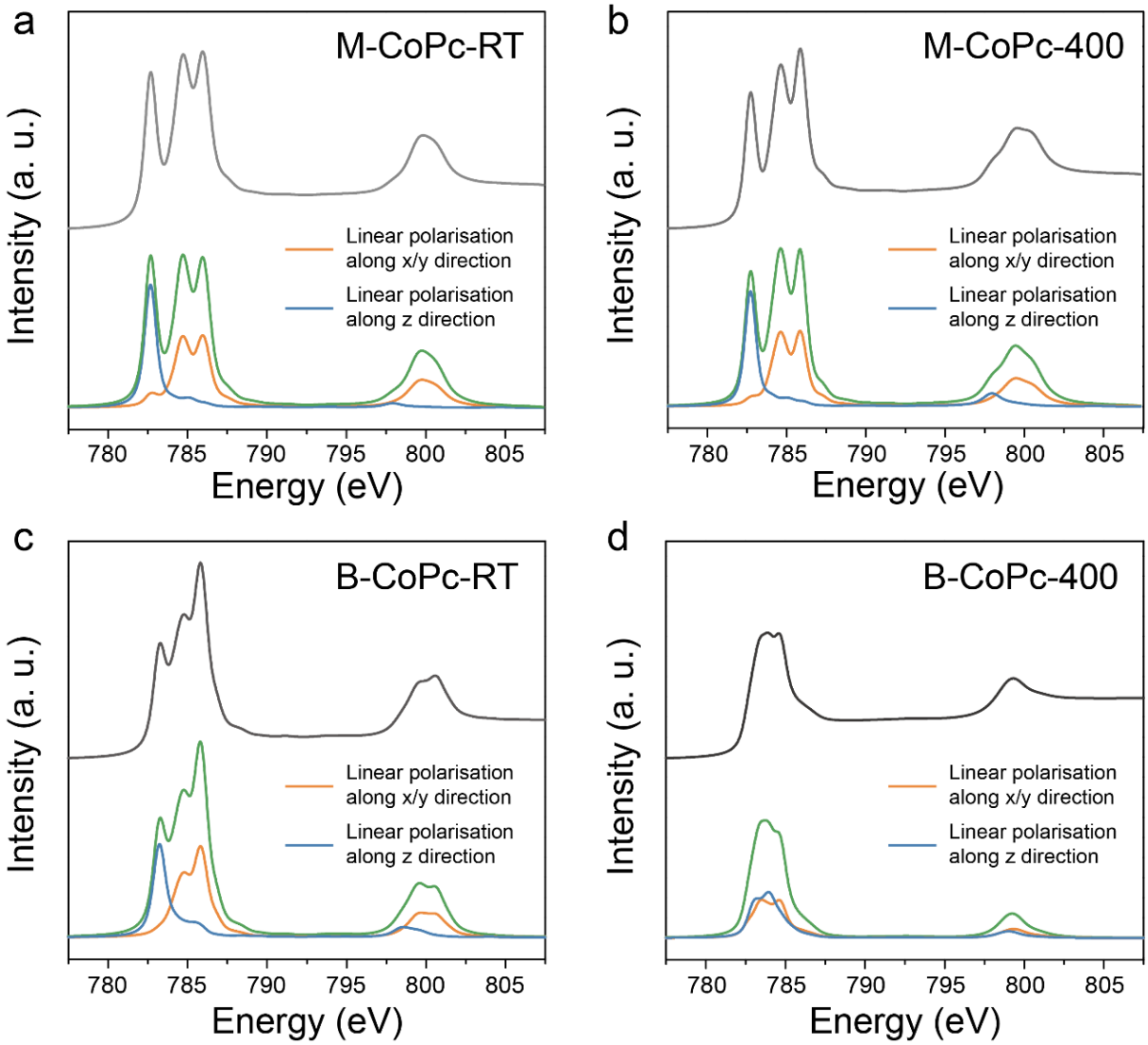


**Figure S17** The simulated X-ray absorption spectra at Co $L_{2,3}$-edge of M-CoPc-RT (a), M-CoPc-RT-400 (b), B-CoPc-RT (c) and B-CoPc-RT-400 (d) at room temperature.

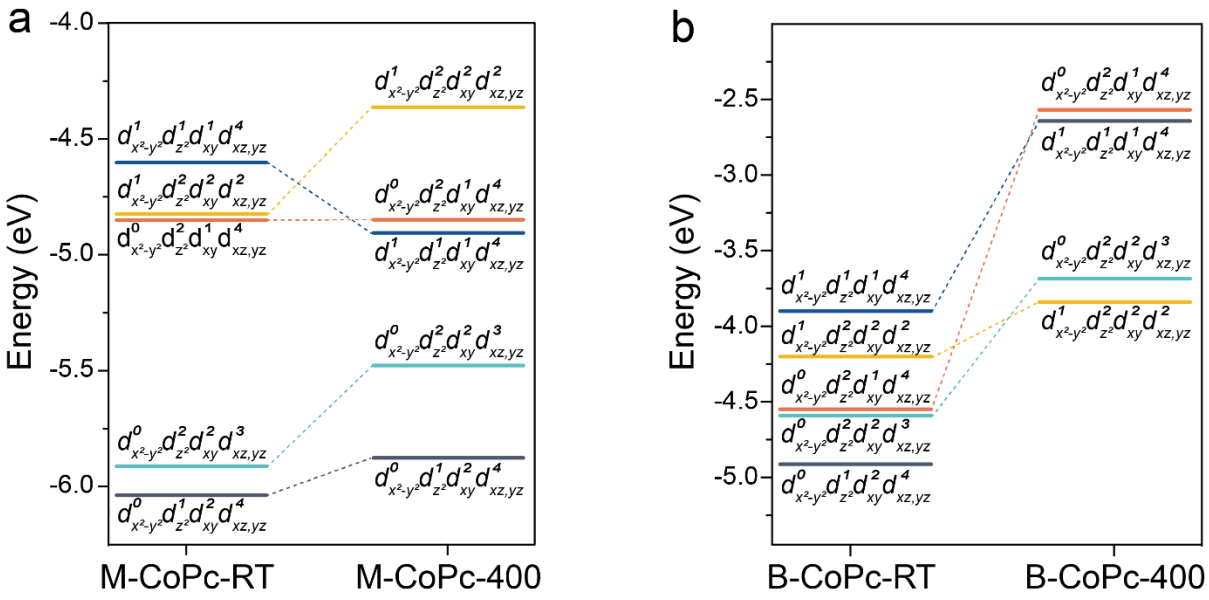


**Figure S18** Energy of the cobalt center in different 3d electron configurations for (a) M-CoPc-RT and M-CoPc-400 as well as (b) B-CoPc-RT and B-CoPc-400.

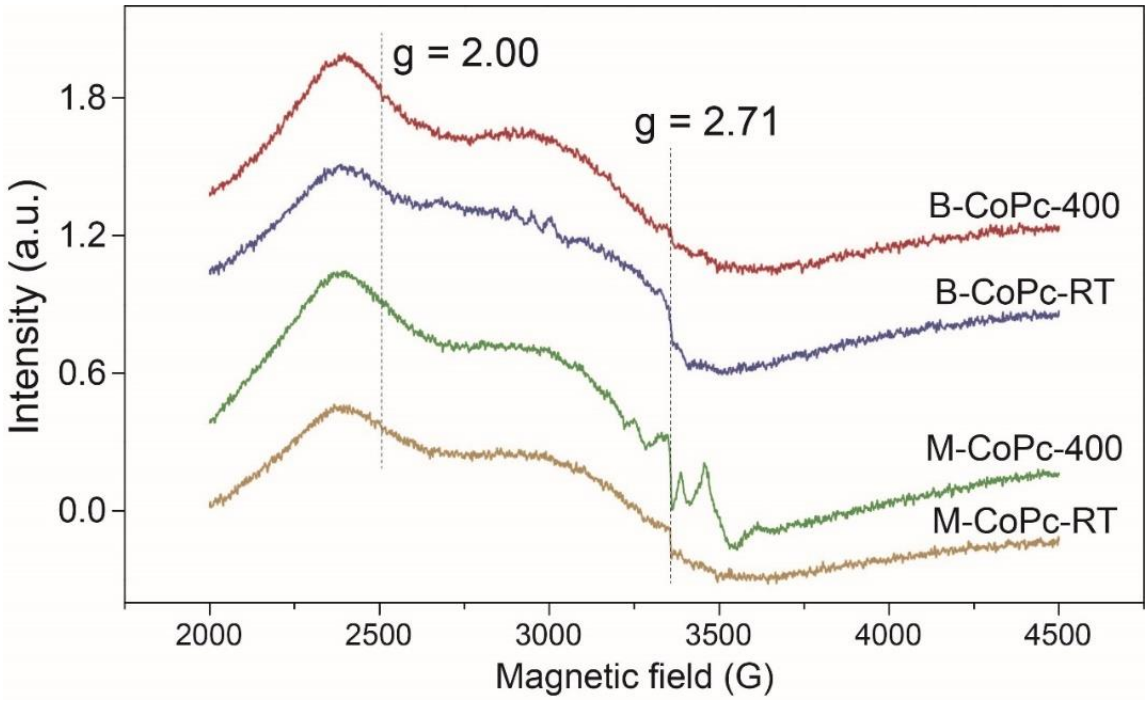


**Figure 19** EPR spectra of various samples.

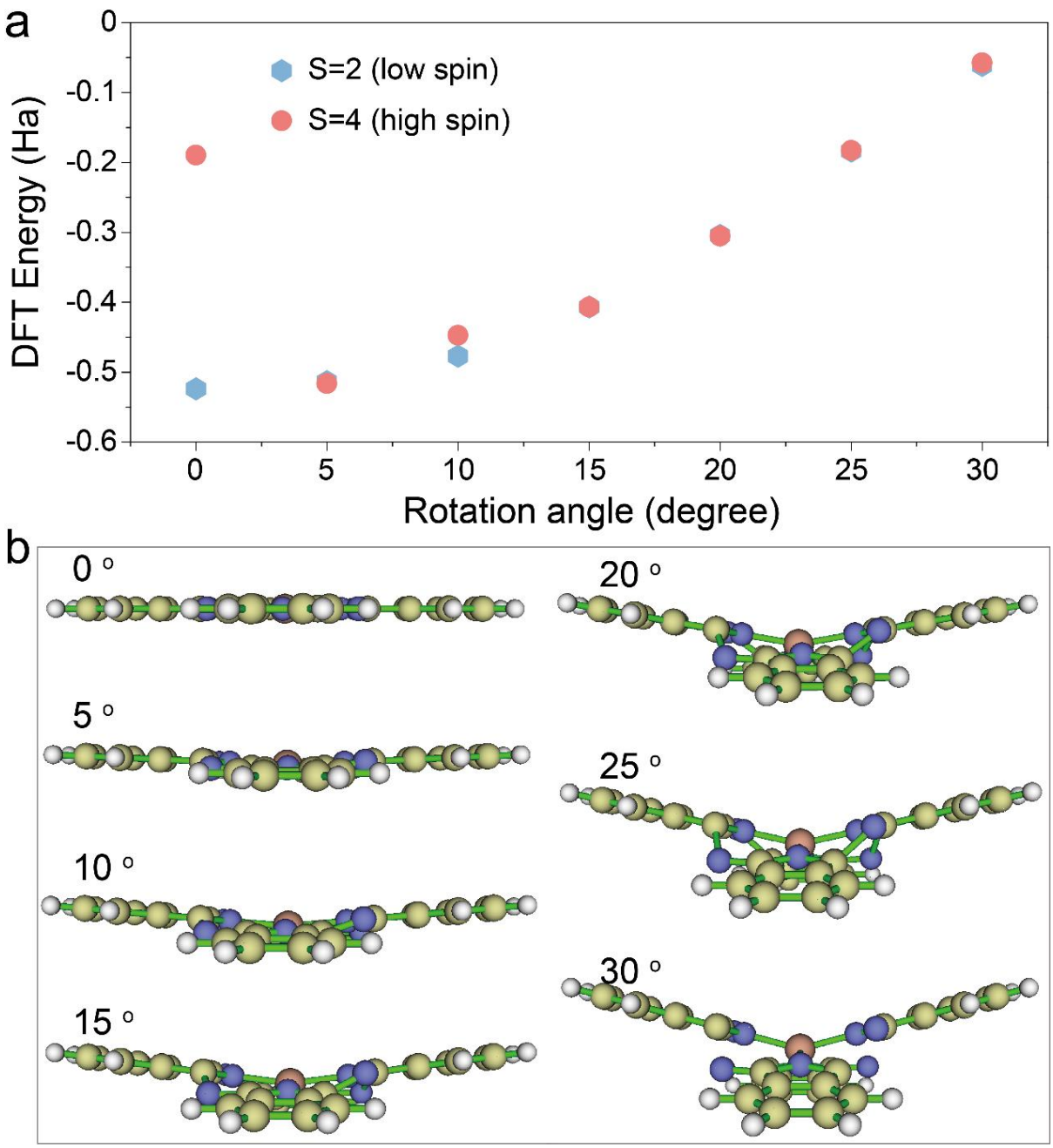


**Figure S20 (**a) The effect of structure distortion on spin state of $Co^{2+}$ in CoPc. (b) The optimized structure of LS-Co and HS-Co with different rotation angles.

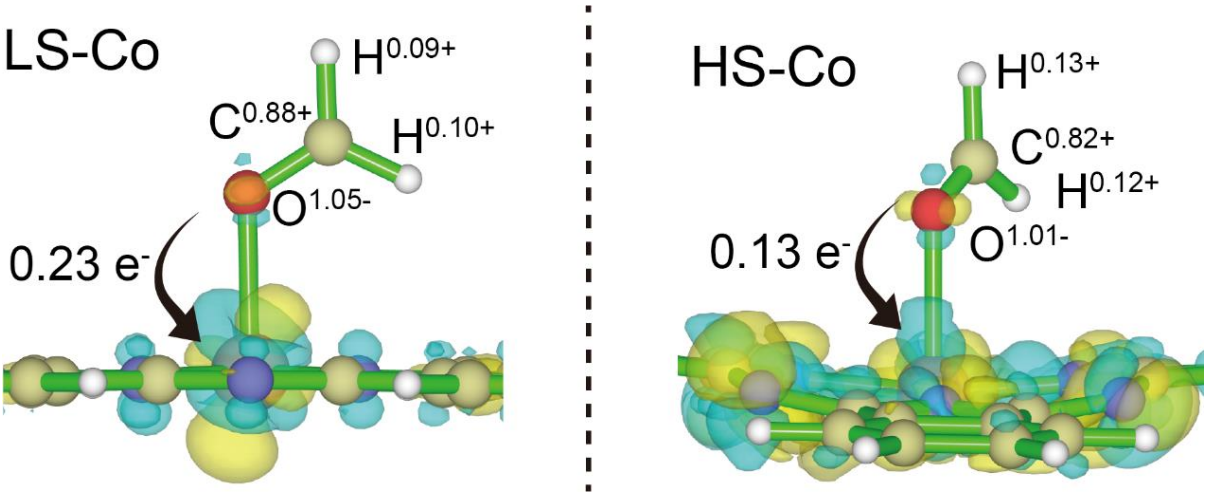


**Figure S21** Schematic illustration showing the *$CH_2O$ adsorption on Co center of LS-Co and HS-Co. Blue, yellow, pink, gray and white balls represent N, C, Co, O and H atoms, respectively, and the faint yellow and cyan regions refer to the increased and decreased charge density.

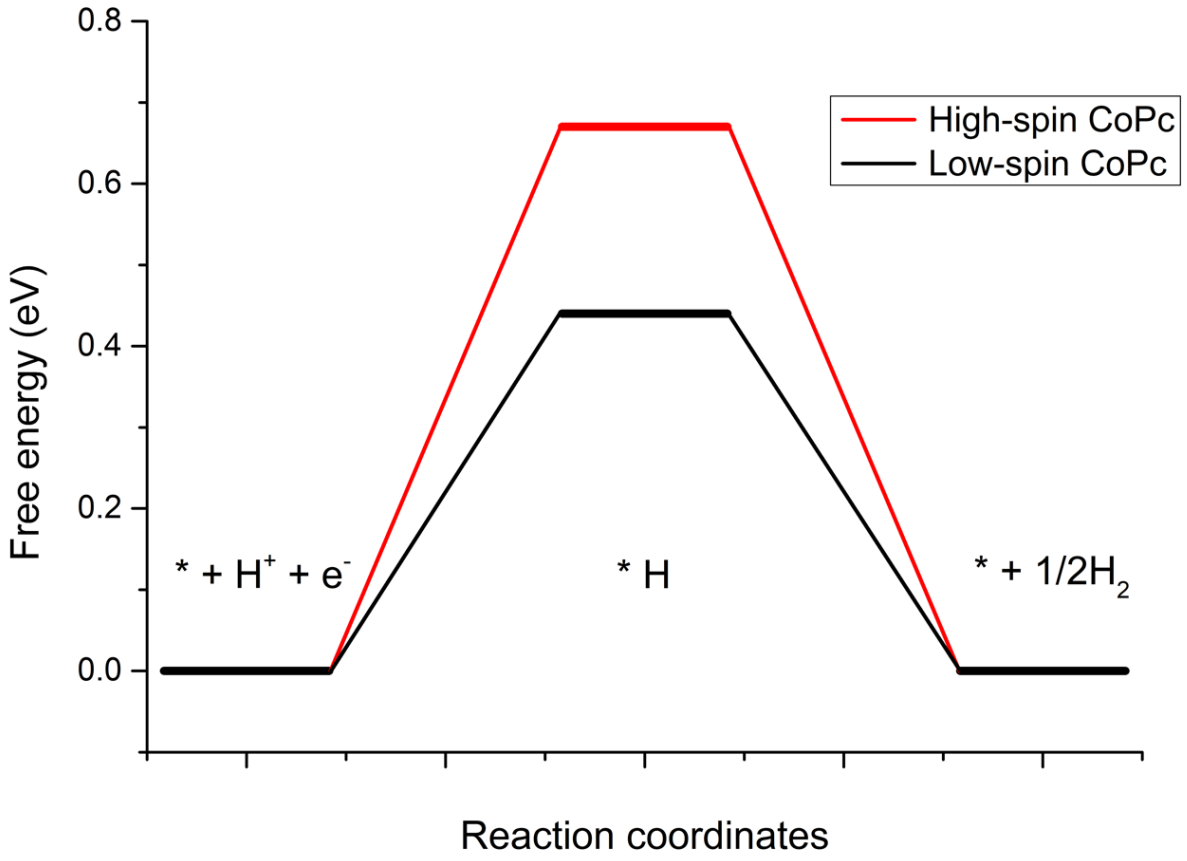


**Figure S22** Potential energy profiles for HER over LS-Co and HS-Co.

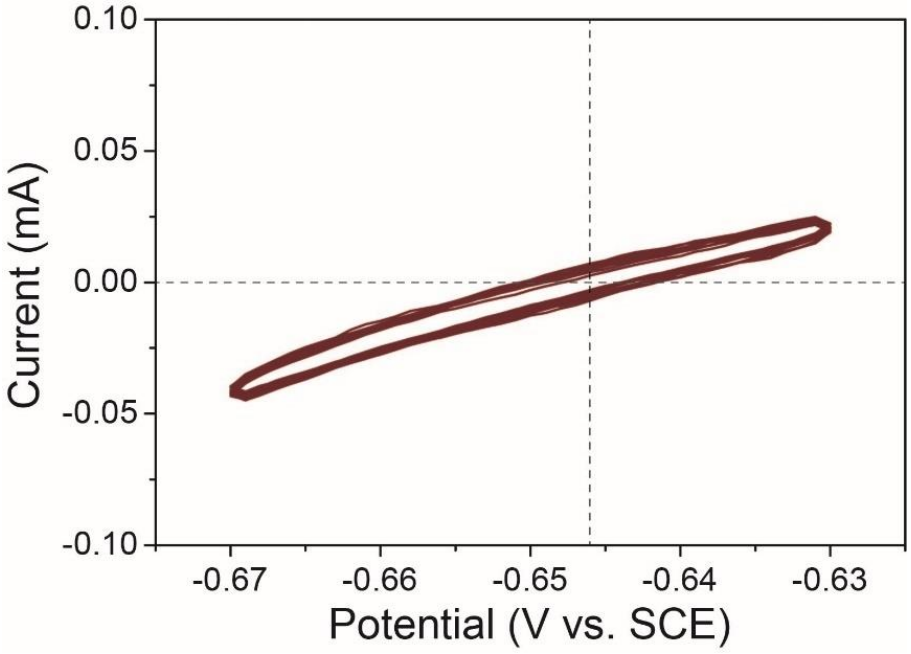


**Figure S23** Cyclic voltammograms of Pt electrode at a scan rate of 1 mV/s in $H_2$ saturated 0.1 M KCl solutions.

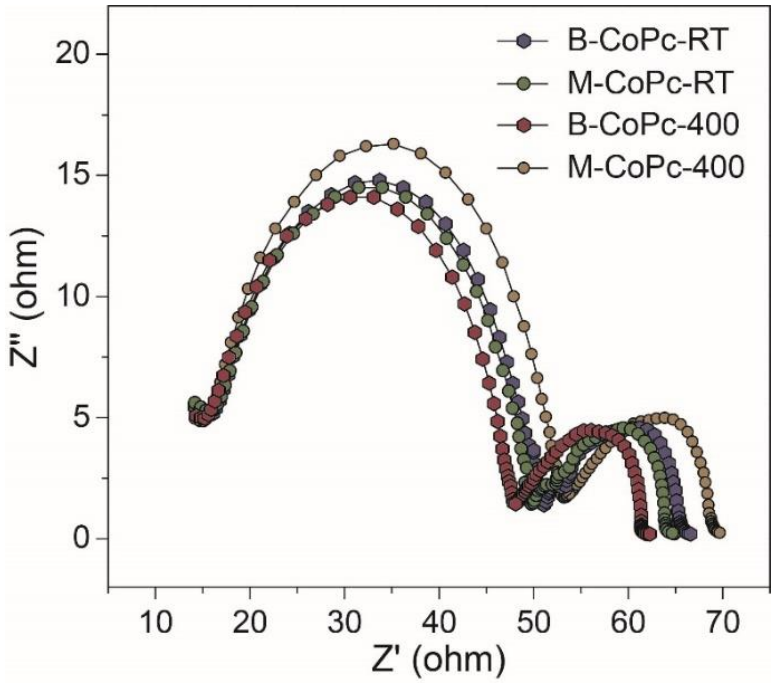


**Figure S24** The EIS spectrum for M-CoPc-RT/400 and B-CoPc-RT/400.

**Table S1.** Structural parameters extracted from the Co K-edge EXAFS fitting. ($S_0^2$=0.76).

| *Sample* | *Scattering pair* | *CN* | *R(Å)* | $\sigma^2(10^{-3}Å^2)$ | $\Delta E_0$*(eV)* | *R factor* ($10^{-2}$) |
|---|---|---|---|---|---|---|
| M-CoPc-RT | Co-N | 4.2 | 1.89 | 3.0 | 3.4 | 6.7 |
| M-CoPc-400 | Co-N | 4.7 | 1.87 | 3.0 | -6.2 | 5.4 |
| B-CoPc-RT | Co-N | 4.7 | 1.92 | 8.0 | -8.1 | 1.8 |
| B-CoPc-400 | Co-N | 4.1 | 2.10 | 5.4 | 1.4 | 1.6 |
| | Co-N | 0.6 | 1.90 | 5.4 | 1.4 | 1.6 |

For the EXAFS fitting in Table S1, $S_0^2$ is the amplitude reduction factor; CN is the coordination number; *R* is interatomic distance (the bond length between Fe and Mo central atoms and surrounding coordination atoms); $\sigma^2$ is Debye-Waller factor (a measure of thermal and static disorder in absorber-scatterer distances); $\Delta E_0$ is edge-energy shift (the difference between the zero kinetic energy value of the sample and that of the theoretical model). *R* factor is used to value the goodness of the fitting.

$S_0^2$ This value was fixed during EXAFS fitting, based on the known structure of Co foil.

Error bounds that characterize the structural parameters obtained by EXAFS spectroscopy were estimated as N ± 20%; *R* ± 1%; $\sigma^2$ ± 20%; $\Delta E_0$ ± 20%.

**Table S2.** FE of all the products.

| Catalysts | Potential (V vs. RHE) | FE($H_2$) | FE($CH_3OH$) | FE (total) |
|---|---|---|---|---|
| M-CoPc-400 | -0.4 | 48% | 5% | 53% |
| | -0.5 | 74% | 11% | 85% |
| | -0.6 | 78% | 13% | 91% |
| | -0.7 | 75% | 19% | 94% |
| | -0.8 | 80% | 16% | 96% |
| | -0.9 | 92% | 1% | 93% |
| | -1.0 | 93% | 2% | 95% |
| B-CoPc-400 | -0.4 | 35% | 8% | 43% |
| | -0.5 | 43% | 44% | 87% |
| | -0.6 | 33% | 57% | 90% |
| | -0.7 | 38% | 56% | 94% |
| | -0.8 | 44% | 48% | 92% |
| | -0.9 | 90% | 4% | 94% |
| | -1.0 | 92% | 2% | 94% |

**Table S3.** Comparison of CORR performance between our prepared catalyst and those reported in the literature.

| Catalyst | Current density (mA) | $FE_{methanol}$ (%) | Reference |
|---|---|---|---|
| B-CoPc-400 | 154 | 57 | **This work** |
| CoPc | 4.77 | 14.3 | *Angew. Chem. Int. Ed.* 2019, 58, 16172 |
| CoPc/MWCNT | 3.8 | 14 | *Chem. Eur. J.* 2022, 28, e202200697 |